Global and Planetary Change 228 (2023) 104210

Contents lists available at ScienceDirect

Global and Planetary Change

journal homepage: www.elsevier.com/locate/gloplacha

Picea schrenkiana tree ring blue intensity reveal recent glacier mass loss in High Mountain Asia is unprecedented within the last four centuries

Weipeng Yue [a], Kristina Seftigen [c,d], Feng Chen [a,b,f,*], Rob Wilson [e], Heli Zhang [a,f], Yunling Miao [g], Youping Chen [a], Xiaoen Zhao [a,b]

[a] Yunnan Key Laboratory of International Rivers and Transboundary Eco-Security, Institute of International Rivers and Eco-Security, Yunnan University, Kunming, China
[b] Southwest United Graduate School, Kunming, China
[c] Regional Climate Group, Department of Earth Sciences, University of Gothenburg, Gothenburg, Sweden
[d] Dendrosciences, Swiss Federal Institute for Forest Snow and Landscape Research WSL, Birmensdorf, Switzerland
[e] School of Earth & Environmental Sciences, University of St. Andrews, St. Andrews, UK
[f] Key Laboratory of Tree-ring Physical and Chemical Research of the Chinese Meteorological Administration/Xinjiang Laboratory of Tree-ring Ecology, Institute of Desert Meteorology, Chinese Meteorological Administration, Urumqi, China
[g] Urumqi Meteorological Bureau, Urumqi, China

ARTICLE INFO

Editor: Dr. Jed O Kaplan

Keywords:
Tree rings
Blue intensity
Glacier mass balance
Tianshan No.1 glacier
Climate change

ABSTRACT

Studies on long-term fluctuations in glacier volume and mass are crucial for understanding past climate change. In this paper, we utilized *Picea schrenkiana* to develop a 525-year chronology of latewood blue intensity (LWBI) in the Tianshan Mountains. Relying on temperature as the main controlling factor for tree growth and glacier mass balance (GMB) variations, the LWBI chronology was used to reconstruct the summer temperature (JJA, R^2_{adj} = 47%) and the annual glacier mass balance (annual GMB, R^2_{adj} = 39%) in the Tianshan Mountains over the past 400 years. The reconstruction results show that the rapid warming since 1974 has caused the Tianshan No.1 glacier (TS No.1) to experience an unprecedented melting trend within the last four centuries. It is disturbing that the glacier still remain in an ablation state for the next 80 years under both representative concentration paths (RCP) 4.5 and 8.5 scenarios, which will exacerbate the adverse environmental impacts of glacial hazards. Our study provides a continuous record for glacier research in high mountains Asian and contributes to a more detailed assessment of glacier and climate change in this region.

1. Introduction

Current climate change is likely to have a serious negative impact on the natural and social systems (Joel and Anne, 1998; Adger et al., 2003; Simpson et al., 2021). Glaciers, as a crucial monitoring indicator of climate change, exhibit an accelerated loss trend due to global warming, characterized by volume reduction, retreat of glacier termini, and thinning (Unger-Shayesteh et al., 2013; Li et al., 2019; Yang et al., 2019). This not only accelerates sea level rise but also significantly affects regional hydrological cycles (Dyurgerov, 2003; Shi et al., 2007; Wang et al., 2013; Radić and Hock, 2014; Chen et al., 2022b). The response of glacial dynamics to climate change is spatially heterogeneous, resulting in varying rates of ice loss across regions and even among glaciers within the same region (Fujita and Nuimura, 2011; Sakai and Fujita, 2017; Dehecq et al., 2019; Wang et al., 2019). Limited observational data and monitoring technology severely restrict our understanding of glacier changes over a longer-term perspective (Salzmann et al., 2014). Glacier mass balance (GMB), which quantitatively reflects the balance between glaciers accumulation and ablation, directly represents the relationship between climate and glaciers (Rabatel et al., 2013). Unfortunately, the global monitoring record of GMB is limited, and little data exists before the 21st century (Braithwaite, 2002; Zemp et al., 2009). The Tianshan No.1 glacier (TS No.1, 43°07′ N and 86°48′ E) in the Urumqi river source region of Xinjiang, China, serves as a benchmark glacier for long-term quantitative monitoring in the area (Fig. 1a/1b) (Wang et al., 2014). It is also the sole reference glacier for assessing glacier mass balance changes in Central Asia (China) by the World Glacier Monitoring Service (WGMS). GMB

* Corresponding author at: Yunnan Key Laboratory of International Rivers and Transboundary Eco-Security, Institute of International Rivers and Eco-Security, Yunnan University, Kunming, China.
E-mail addresses: feng653@163.com, 20190012@ynu.edu.cn (F. Chen).

https://doi.org/10.1016/j.gloplacha.2023.104210
Received 30 October 2022; Received in revised form 16 July 2023; Accepted 30 July 2023
Available online 1 August 2023
0921-8181/© 2023 Published by Elsevier B.V.

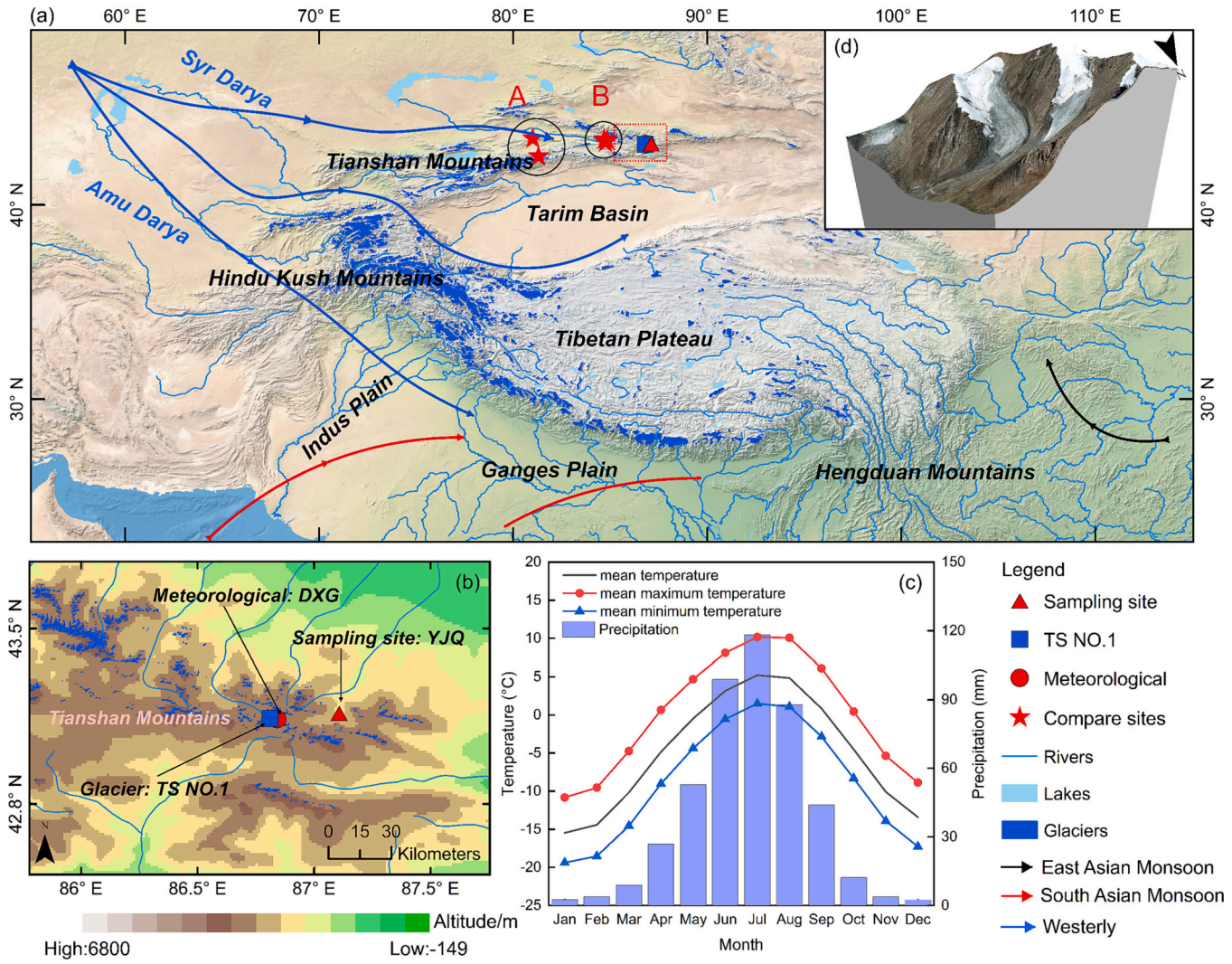

Fig. 1. Overview of the study area, (a) the geography of the high mountains Asian, (b) the locations of the sampling site (YJQ), the glacier (TS No.1, 43°07′ N and 86°48′ E) and meteorological station (DXG, 43°03′ N and 86°30′ E), (c) monthly temperature and total precipitation recorded at the DXG meteorological station (1959–2016 period), (d) a three-dimensional satellite image of the TS No.1 glacier. The red dotted box in (a) indicates the geographical range of subgraph (b). The locations of sampling sites based on MXD temperature reconstruction for comparison with this study are from Chen et al. (2019b, A) and Yu et al. (2013, B). (For interpretation of the references to colour in this figure legend, the reader is referred to the web version of this article.)

changes have been continuously monitored for more than half a century (1959 – present), providing valuable data for glacier research (Gao et al., 2018). Due to its proximity to the city of Urumqi, waste heat and dust aerosols released by human activities are considered to be the main drivers of the rapid melting of TS No.1 glacier since the 1980s (Wang et al., 2014; Yue et al., 2017). But how did the TS No.1 glacier change before the 20th century? Will the ablation trend persist into future decades? To answer these questions, we need reliable proxy data to assess its historical changes and provide underlying baseline data to help with future simulations.

Accurately dated and well replicated tree ring chronologies can provide robust reconstructions of past climate at multi-centennial scales (Liang et al., 2008; Fan et al., 2009; Cook et al., 2010; Maxwell et al., 2011; Yang et al., 2014; Gou et al., 2015; Chen et al., 2019a; Liu et al., 2020). Tree-ring maximum latewood density (MXD) and stable isotopes are critical for expanding and enhancing the coverage of temperature or moisture sensitive tree-ring records. (Büntgen et al., 2006; Gagen et al., 2011). However, the expensive technical cost and complex operational steps for measuring cell density and stable isotope means that these methods are only applied in a few laboratories and limited number of studies (Cao et al., 2020). In contrast, the blue intensity (BI) parameter, which is based on light reflectance, offers a more affordable and accessible option for any tree-ring laboratory (Björklund et al., 2014; Wilson et al., 2017; Seftigen et al., 2020; Heeter et al., 2021a; Davi et al., 2021; Kaczka and Wilson, 2021). By measuring the intensity of the reflectance of blue light from scanned tree-ring images, BI provides a measure of the relative density in tree rings (Rydval et al., 2014; Dolgova, 2016; Fuentes et al., 2018; Björklund et al., 2019; Cao et al., 2020; Harley et al., 2021; Davi et al., 2021; Heeter et al., 2021b). Depending on the conifer species, however, there can be a distinct colour difference between the heartwood (HW) and sapwood (SW) which can bias long term trends (Fuentes et al., 2018; Cao et al., 2020; Tsvetanov et al., 2020; Harley et al., 2021; Cao et al., 2022). For this study, we utilize samples from *Picea schrenkiana*, which expresses relatively small colour difference and is a good candidate species for BI measurement therefore.

Samples of *Picea schrenkiana* were collected near TS No.1 glacier and analysed for BI. By analysing the relationship between long-term tree ring BI and GMB, our goal is to reconstruct the historical changes of the TS No.1 glacier; understand the process characteristics of its changes; assessing the present state of glacier change within the context of the past few centuries and predicting the future trend of glacier change. Ultimately this work will provide an important long-term empirical

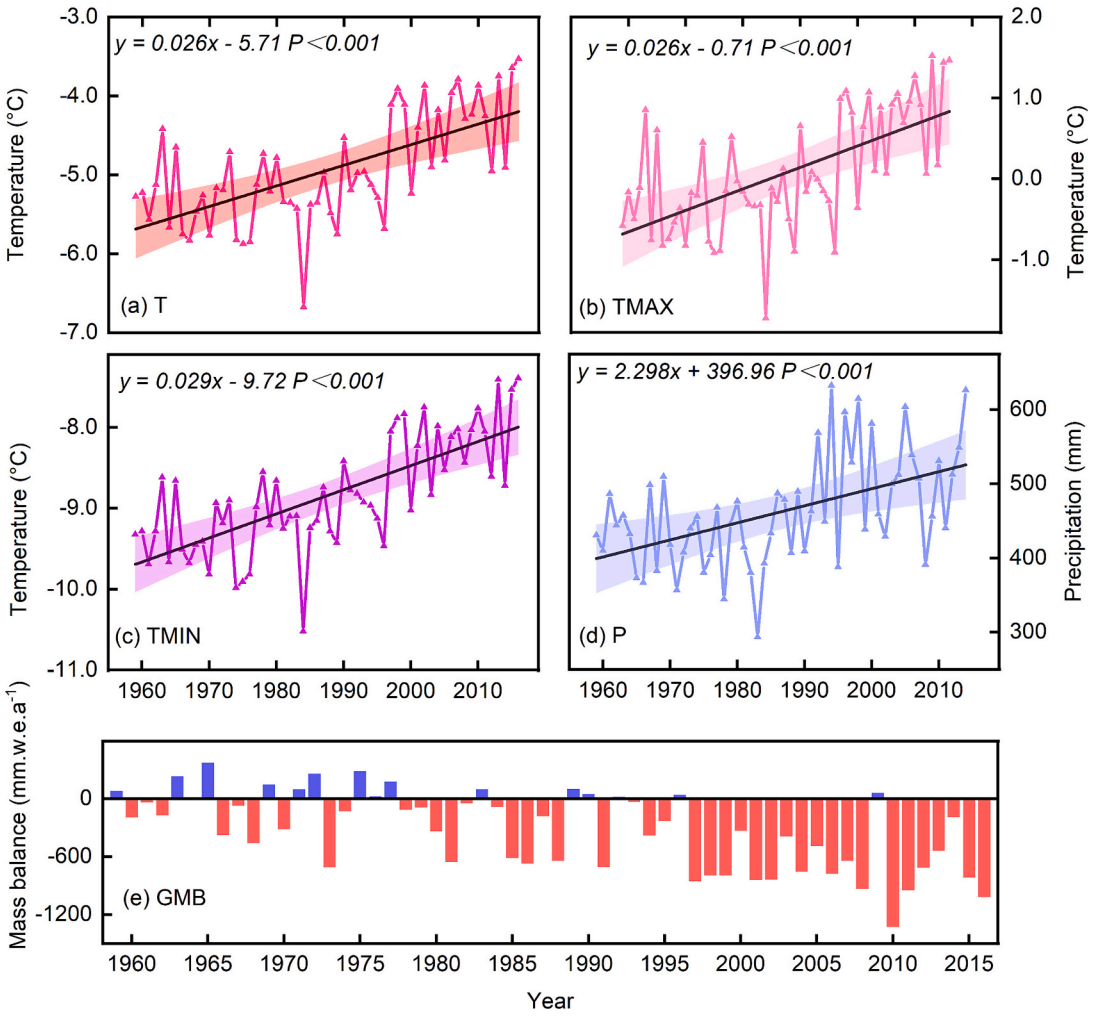

Fig. 2. The linear regression trends, along with 99% confidence bands, for annual mean temperature (T, a), annual mean maximum temperature (TMAX, b), annual mean minimum temperature (TMIN, c), and annual total precipitation (P, d) measured at the Daxigou meteorological station. Monitored glacier mass balance data of the TS No.1 glacier (GMB, e). All records span the time period from 1959 to 2016.

Table 1
Tree-ring sampling sites and meteorological stations.

Site	Lat.(N)	Long.(E)	Elevation (m)	Aspect	Slope	Cores/Trees	Species
YJQ	43°08′	87°06′	3054	S	20–40°	52/37	*Picea schrenkiana*
DXG	43°03′	86°30′	3539	n/a	n/a	n/a	n/a
TS NO.1	43°07′	86°48′	3896	n/a	n/a	n/a	n/a

basis for further glacier research in high mountain Asia.

2. Materials and methods

2.1. Study area and sample collection

The study area (42° – 44° N and 86° – 88° E) is situated in the hinterland of the Asian continent, the central Tianshan Mountains (Fig. 1a). The landscape of the study area is characterized by a coniferous forest belt that is replaces at higher elevations (2900 m a.s.l.) by grasslands and finally by bare rocks and glaciers at the highest elevations (3700 m a.s.l.) (Zhang et al., 2019; Chen et al., 2022b). Meteorological records from Daxigou (DXG, 43°07′ N and 86°48′ E, 3896 m a.s.l, 1959–2016, 20.9 km from the sampling site), the high-altitude area of central Tianshan mountains has an annual mean temperature of −5 °C, and temperatures of 5.2 °C and − 15.5 °C in the warmest (July) respective coldest (January) months of the year. The total annual precipitation sums up to 462.4 mm, which of 66% falls in the summer season (Fig. 1c). Over the past six decades, the central Tianshan Mountains have witnessed a gradual shift towards a warmer and wetter climate regime. The temperature (including mean temperature, mean maximum temperature, and mean minimum temperature) has increased at a rate exceeding 0.25 °C per decade, while the precipitation has increased at a rate of 22 mm per decade (Fig. 2). GMB monitoring of the TS No. 1 glacier reveals that it has been in a state of a retreat for over 30 years (Fig. 2).

Our sampling site is located in the headwaters of the Urumqi River basin in the Central Tianshan mountains (YJQ, 43°08′ N and 87°06′ E, 3054 m a.s.l., Fig. 1, Table 1). Using an increment borer, we collected 10 mm diameter tree-ring cores from living *Picea schrenkiana* (Schrenk's spruce) individuals (Chen et al., 2022a). A total of 65 increment cores were collected from 37 dominant, old-looking trees growing across the upper treeline. The microenvironmental conditions around the sampled

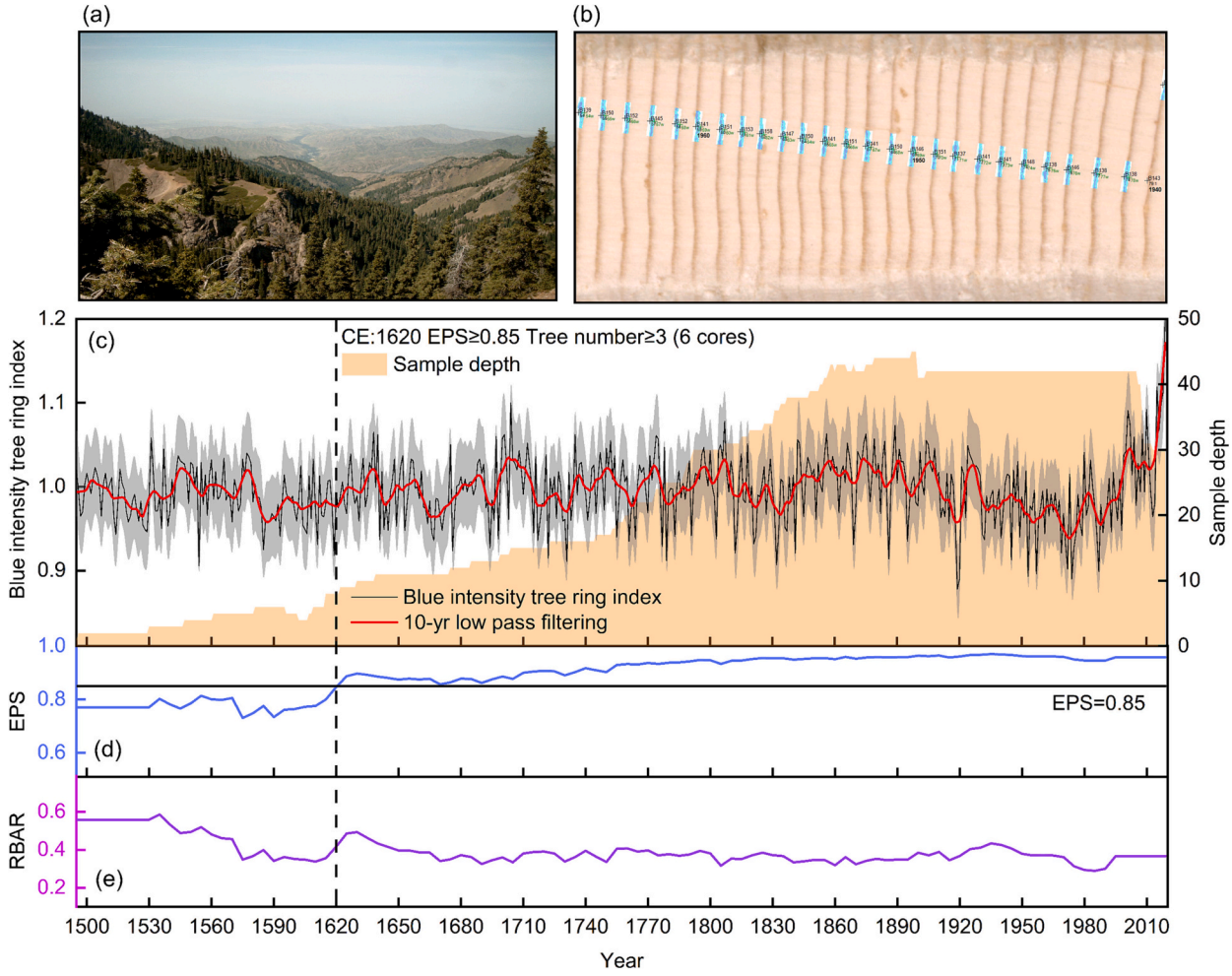

Fig. 3. (a) A photo of the sampling site in the Central Tianshan mountains. (b) The CooRecorder software used to measure the blue light reflectance of latewood. (c) The tree-ring latewood blue intensity standard chronology (LWBI, thin black line), smoothed with a 10-year low-pass filter (red thick line). Grey shading highlights the ±10% error of the un-smoothed LWBI chronology, while the orange fill shows how the sample depth (No. of cores) changes through time. (d) Expressed population signal (EPS) (computed over 50 years, lagged by 45 years), and (e) mean inter-series correlation (Rbar) statistics. The EPS > 0.85 threshold is outlined by the vertical dashed line. (For interpretation of the references to colour in this figure legend, the reader is referred to the web version of this article.)

Table 2
Tree-ring blue intensity chronologies statistics.

Parameter	MS	SD	SNR	MC	VFE	AOF	EPS	MSC	EPS ≥ 0.85
YJQ	0.06	0.36	21.34	0.60	45.4%	0.96	0.95	1495–2019	1620

Note: MS is mean sensitivity, SD is standard deviation, SNR is signal to noise ratio, MC is mean correlation with master series, VFE is variance in first eigenvector, AOF is autocorrelation order first, EPS is expressed population signal, MSC is master series coverage.

individuals were characterized by poor soils, steep hillsides, and a high abundance of fractured rocks (Fan et al., 2009; Li et al., 2015; Rao et al., 2020) (Fig. 1b and Table 1). The sampling site experiences relatively cool summers and short growing season, indicating that the growth of *Picea schrenkiana* across the tree line is highly sensitive to growing season temperatures (Chen et al., 2012).

2.2. Chronology development

In the laboratory, the samples were carefully examined and those cores that showed signs of fungal decay, discoloration, traumatic resin duct formation or any other abnormal features were removed from further analysis (Björklund et al., 2014). This pre-screening process retained 52 cores from a total of 37 trees for the BI measurements. To remove resin and extractives, the tree cores were first washed in hot ethanol for 48 h using a Soxhlet apparatus, and then in boiling deionized water to remove any residual solvent and water-soluble extract (Poole, 2020; Khan et al., 2022). Subsequently, the samples were fixed, air dried, and finally sanded with progressively finer sandpaper (from 400 to 1000 grit) to achieve a smooth core surface and distinct ring boundaries (Schweingruber, 2012).

A calibrated standard flatbed scanner (Epson Expression 12000XL) was used to scan each core at a 3200-dpi resolution. Ring width, as well as the blue light reflectance of the latewood (LWBI) portion of the ring were measured in the CooRecorder 9.4 software (Larsson, 2018) (Fig. 3b), and verified for cross-dating accuracy in program COFECHA (Grissino-Mayer, 2001). Compared with the earlywood, the latewood avoids colour differences from the lighter sapwood (SW) to darker heartwood (HW) as *Picea schrenkiana* (Buckley et al., 2018; Seftigen et al., 2020). The raw LWBI is here defined as the mean of the darkest

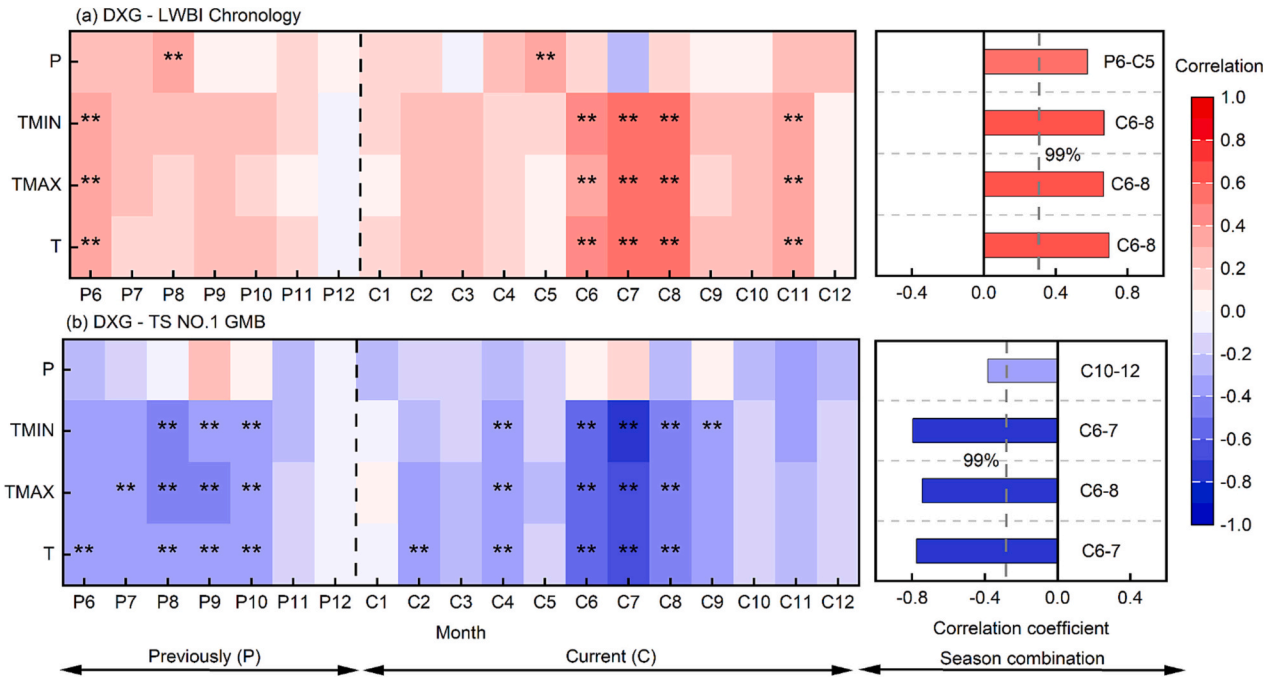

Fig. 4. (a) Correlations between meteorological data and the LWBI chronology (a), annually resolved TS No.1 GMB observations (b). Correlation is computed over the 1959–2016 period. Meteorological data includes mean maximum temperature (TMAX), mean temperature (T), mean minimum temperature (TMIN), and total precipitation (P) of the previous (P6 – P12) and current years (C1 – C12). Correlation coefficients for different monthly combinations are provided in the right plots. ** indicates significant correlations at the 99% confidence level.

30% pixels in latewood (Rydval et al., 2014; Wilson et al., 2017; Cao et al., 2020), and inverted with the formula: LWBI = 2.56 – LWBI (raw)/100. This inversion was performed to ensure that LWBI showed a positive correlation with wood density. One of the main obstacles of the BI measures is that any colour changes across the sample that are not related to the interannual changes in anatomical properties of the wood (e.g., heartwood/sapwood transition, or resin/fungal staining) will inflict a bias in the resulting intensity measures. By subtracting early-wood reflectance values from the latewood reflectance values, Björklund et al. (2014) demonstrated that such heartwood/sapwood colour changes could be mitigated (Delta blue intensity, DBI) (Wang et al., 2020). In the current study, the *Picea schrenkiana* samples showed no sharp or pronounced colour transition from the heartwood to the sapwood in the latewood reflectance values. Hence, we here proceeded using the latewood blue intensity parameter (LWBI) (Björklund et al., 2014; Wilson et al., 2014; Fuentes et al., 2018; Cao et al., 2020; Heeter et al., 2021a; Davi et al., 2021; Kaczka and Wilson, 2021; Cao et al., 2022).

The LWBI chronology was developed in ARSTAN program (Cook et al., 2005; Speer, 2010). Individual LWBI series were detrended by applying a linear regression of any slope, and then averaged into a site chronology using the robust weighted mean method (Cook et al., 1995). To reduce the effects of a changing sample size on the variance of the chronology, the variance was stabilized following the method described in Osborn et al. (1997). The quality of the chronology was assessed with the expressed population signal (EPS) and mean inter-series correlation (Rbar) statistics (Wigley et al., 1984). To retain only the reliable portion of the data, the chronology was truncated at 1620 CE according to the arbitrary EPS > 0.85 threshold level, that is, at a sample depth of ≥6 cores (3 trees) (Fig. 3) (Table 2).

2.3. Environmental data

The instrumental meteorological data from the Daxigou meteorological station (covering the period 1959–2016) were obtained from the China Meteorological Data Service Centre (http://data.cma.cn/en). Annually-resolved GMB observations of the TS No.1 glacier, covering the period 1959–2016, were obtained from the National Tibetan Plateau Data Centre (http://data.tpdc.ac.cn) (Xiao and Shangguan, 2018; Zemp et al., 2019; Li et al., 2021). The GMB of TS No.1 glacier was measured according to the glaciological method described by Østrem and Brugman (1966), namely the conventional stake/snow pit method. Gridded (0.5° × 0.5°) mean CRU TS 4.05 temperature data from the Climate Research Unit (https://crudata.uea.ac.uk/cru/data, Harris et al., 2020) and gridded Northern hemisphere snow cover data from the Rutgers University Global Snow Laboratory were used to assess the spatial representativeness of our reconstructions (http://climate.rutgers.edu/snowcover/index.php) (McCabe and Wolock, 2010; Harris et al., 2014). The ERA5 2-m temperature dataset (ECMWF, 0.28° × 0.28°, https://cds.climate.copernicus.eu) was utilized to analyse the association between regionally reconstructed temperature and land-sea temperature, while the Atlantic multidecadal variability (AMV, Wang et al., 2017) index was used to verify the teleconnection mechanism of temperature anomalies between land and sea. To evaluate future changes of the TS No. 1 glacier, the CMIP5 regional downscaling meteorological element data (HadGEM3 model), developed by the National Institute of Meteorological Sciences (NIMS, http://cordex-ea.climate.go.kr/cordex), were used. The configuration of the model domain followed the protocol of the Asian coordinated regional climate downscaling experiment (CORDEX-East Asia) (Baek et al., 2013). From the set of model data, 10 meteorological variables with a horizontal resolution of 0.22° and the spatial domain 42.5° N – 43.5° N and 85.5° E – 88.0° N were selected (Martin et al., 2006; Ringer et al., 2006; van Vuuren et al., 2011) (Table S1). For future climate simulations, two different boundary conditions in the representative concentration pathways 4.5 and 8.5 scenarios (RCP 4.5 and RCP 8.5) were used (Table S1).

2.4. Statistical methods

Response function analysis, performed in the Dendroclim2002 software (Biondi and Waikul, 2004), was used to estimate how the LWBI chronology is linked to climatic variables and GMB. The analysis was

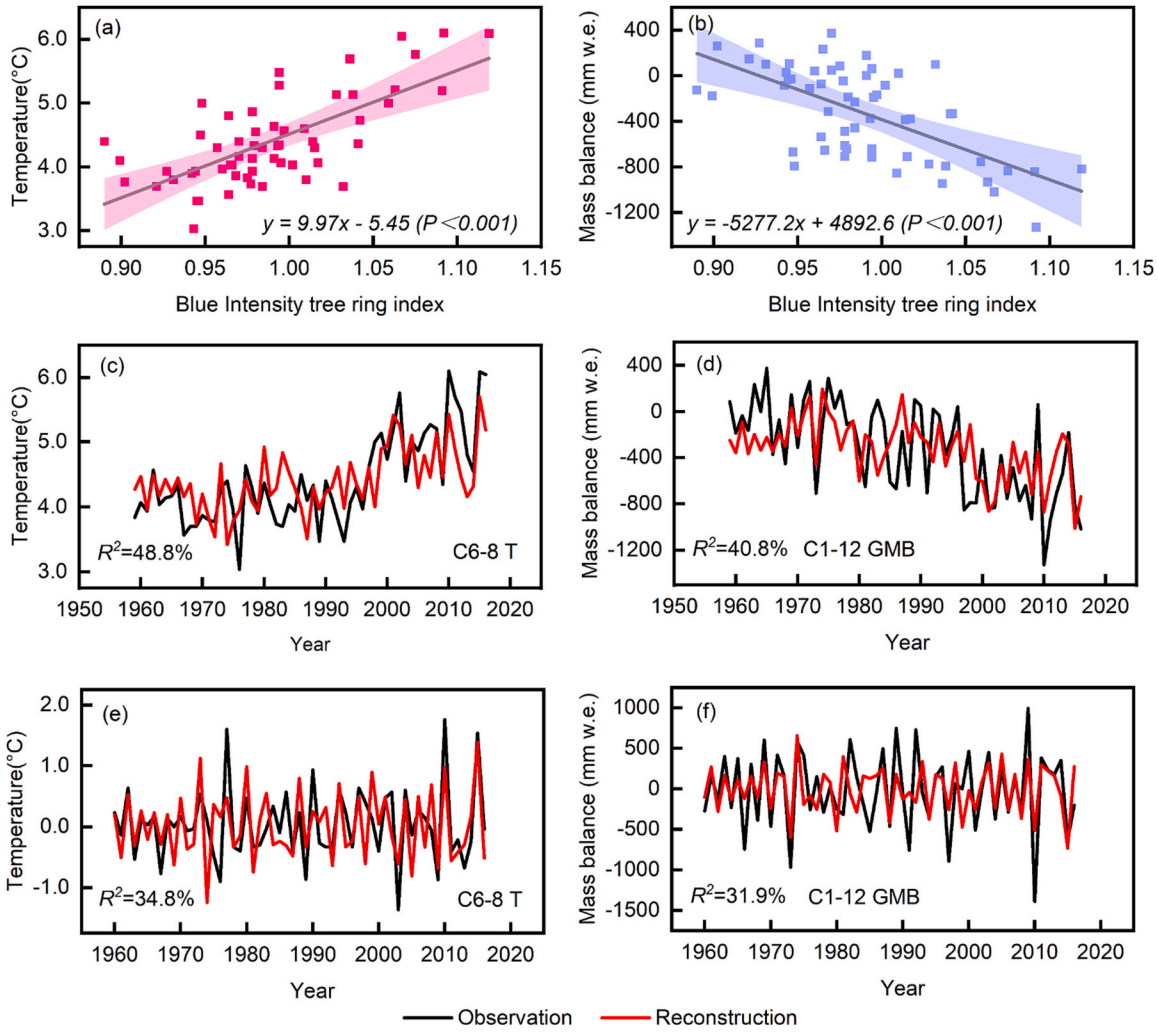

Fig. 5. (a) The linear regression model between the LWBI and the summer mean temperature (June to August). (b) The linear regression model between the LWBI and annual GMB (January to December). The original comparison (c) and first-order difference (e) between the reconstructed and observed summer temperature. The original comparison (d) and first-order difference (f) between the reconstructed and observed annual GMB.

Table 3
Leave-one-out cross-validation statistics for the summer temperature and glacier mass balance reconstructions.

Reconstructed object	Period	R^2	R^2_{adj}	*F*	*r*	*RE*	*PMT*	*ST*	*DW*
Summer temperature	1959–2016	0.48	0.47	53.33**	0.69	0.44	5.58	42+/16-**	1.27
Glacier mass balance	1959–2016	0.40	0.39	38.64**	−0.63	0.36	6.97	41+/17-**	1.69

Note: R^2 is model explained variance, R^2_{adj} is adjusted R^2 considering multiple independent variables in the model, *F* is the statistical significance of the regression models, *DW* is Durbin–Watson test, *r* is correlation coefficient from the leave-one-out cross validation, *RE* is reduction of error, *ST* is sign test, *PMT* is product means test, ** indicate the 99% confidence level.

carried out from June of the previous year to December of the current year, as tree growth is influenced by climatic conditions in the previous and current growing seasons (Fritts, 1976). Further, Spatial correlation analyses between the LWBI chronology and gridded temperature, snow cover, and globally representative glaciers GMB were performed to assess whether the established LWBI chronology contains large-scale climate signals (Chen et al., 2022b). Based on the climate response analysis, a linear regression model was developed, using the observation temperature (or GMB data) as the dependent variable and the LWBI index as the independent variable (Zhang et al., 2019). The skill of each model was evaluated by a leave-one-out cross-validation (Michaelsen, 1987), where the reduction of error (RE), sign test (ST), product mean test (PMT), and Durbin – Watson test (DW) were used to test the validity of the models (Speer, 2010). To analyse the long-term variability, proxy-based estimates were smoothed using a 10-year low-pass filter. Based on the low-pass filtered time-series (LOWESS: local weighted regression method, Cleveland and Devlin, 1988), warm/cold (melt/accumulate) periods were defined as 10 consecutive years above (below) the long-term average (1620–2019 period). Further, according to Liu et al. (2019) the mean ± 1σ (σ is the standard deviation) was used as the threshold for warm/cold (melt/accumulate) years, and the mean ± 2σ was used as the threshold for extremely warm/cold (melt/accumulate) years. For the determination of periodicities, the multi-taper method (MTM) and wavelet power spectrum analysis were employed to cross-validate any periodic signals in the temperature record, along with a red noise test (Mann et al., 2022). The first principal component (PC1), which accounts for the largest total variance, was used in this study to extract common signals from all variables (Briffa et al., 2001).

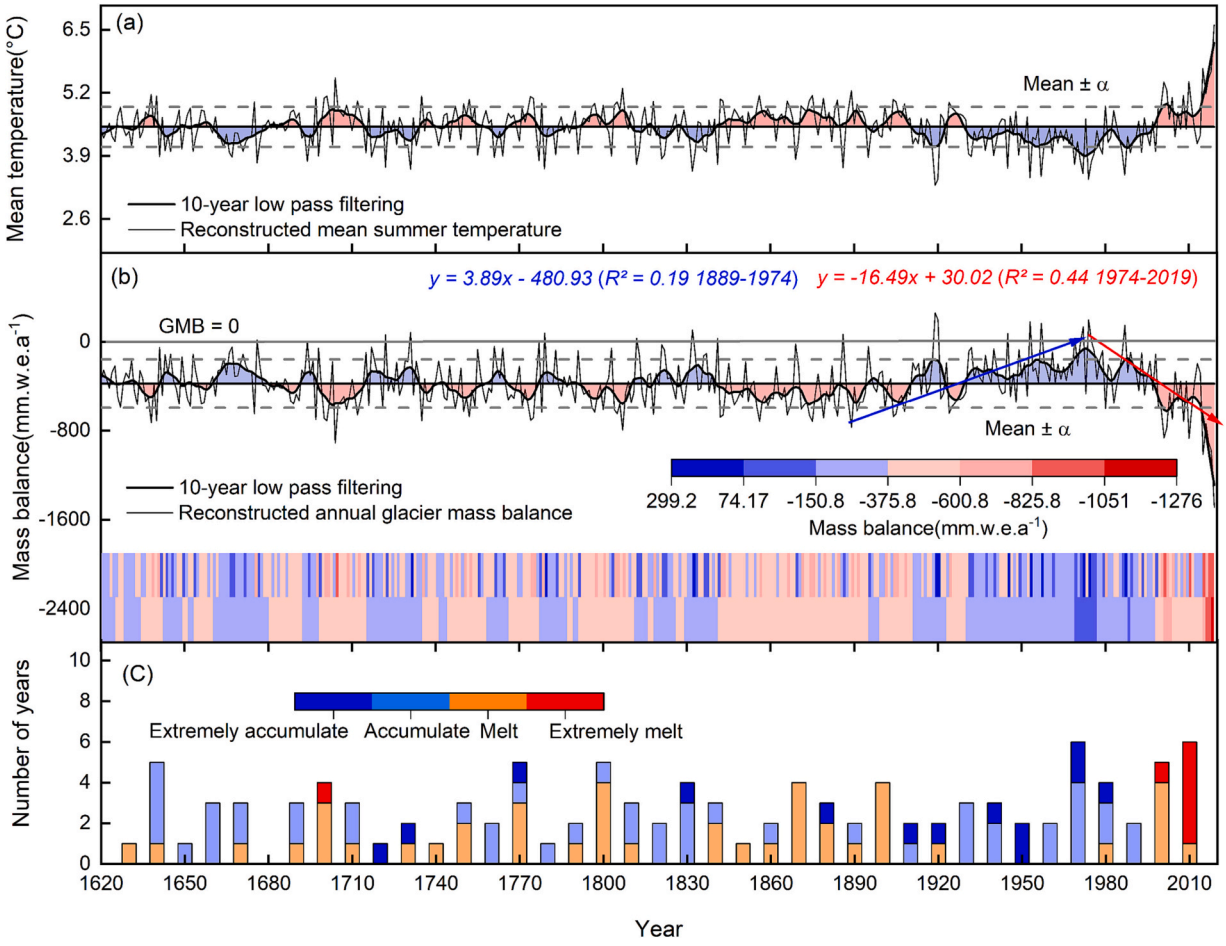

Fig. 6. (a) Reconstructed of summer (June to August) mean temperature in Tianshan since 1620. (b) Reconstructed annual glacier mass balance for the Tianshan No.1 glacier (top), and a colour classification heat map of the reconstructed annual glacier mass balance and its 10-year low-pass filter values over the 1620–2019 CE period (bottom). (c) Distribution of extreme melt and extreme accumulation years per decade of the Tianshan No. 1 glacier over the past 400 years.

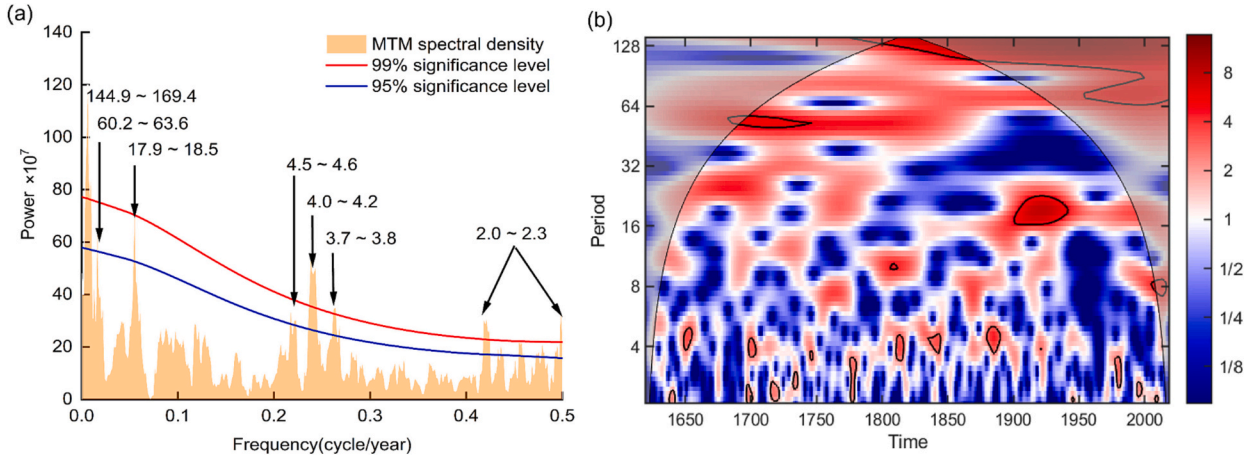

Fig. 7. (a) Power spectral density (MTM analysis) for the reconstructed results (includes summer mean temperature and annual GMB), with the 99% and 95% confidence levels inferred from red noise spectra (periodicities significant at the 99% level are indicated). (b) Wavelet power spectrum of the reconstructed results, with significant periods ($P < 0.01$) highlighted by black lines. (For interpretation of the references to colour in this figure legend, the reader is referred to the web version of this article.)

Furthermore, a multiple linear regression model was established to estimate the future of GMB based on the multi-meteorological elements in the HadGEM3 model, and provide corresponding statistical tests (Soares dos Santos et al., 2016).

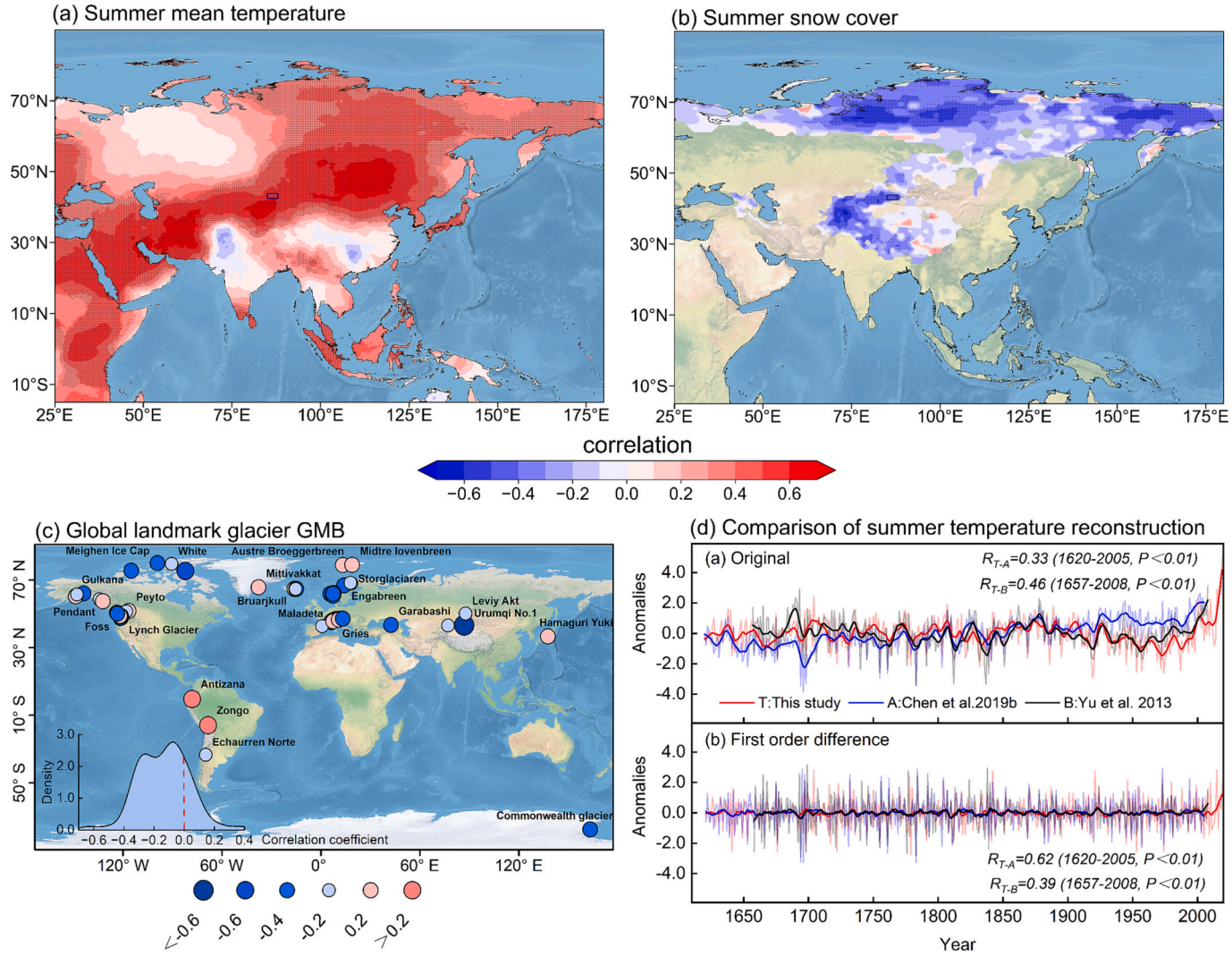

Fig. 8. Point-by-point correlation analysis between the LWBI chronology and (a) gridded CRU JJA temperatures (1950–2019 period), (b) Northern hemisphere JJA snow cover (1966–2019 period), and (c) glacier mass balance data from 76 landmark glaciers around the world. The study area was marked by a black box in (a) and (b), while areas of significant ($P < 0.01$) correlations are shown in colour. The lower left plot in (c) displays the distribution density of the correlation coefficients between LWBI and the 76 landmark glaciers. (d) The current summer temperature reconstruction is compared with the Tianshan summer temperature reconstruction from Chen et al., 2019b (June to August) and Yu et al., 2013 (May to August). The latter two reconstructions are based on *P. schrenkiana* MXD, derived with the X-ray technique. All reconstructions are normalized over the common period, and filtered using a 10-year low-pass filter.

3. Results

3.1. Climate and glacier responses

The correlation analysis reveals significant positive associations between the LWBI chronology and summer (June – August) and late autumn (November) temperatures of the current year, as well as June of the previous year. Albeit weaker than with temperature, the LWBI chronology also show a significant positive correlation with precipitation in late summer (August) of the previous year and late spring (May) of the current year (Fig. 4a). Among the various monthly combinations, the correlation between the LWBI chronology and mean temperatures for June – August is the strongest ($r = 0.698$, $P < 0.01$). The response pattern of the DBI chronology to climate was also tested (Fig. S1), showing a similar pattern to LWBI but with a weaker correlation coefficient, indicating that LWBI is more sensitive to temperature response. Further, our results show, as expected, that the annual GMB of the TS No.1 glacier is significantly negatively influenced by temperatures both of the current and previous years, and especially so to June through August temperatures of the current year. The strongest correlations between the annual glacier ice mass balance of the TS No.1 and temperature are found for the mean minimum temperature during the June – July season ($r = -0.797$, $P < 0.01$) (Fig. 4b). Notably, there is no significant relationship found with annual GMB data over the 1959–2016 period and precipitation.

3.2. Reconstruction of summer temperature and annual glacier mass balance

We show that warm season temperature is the key controlling factor of *P. schrenkiana* latewood density (i.e., LWBI). In parallel, we find a strong negative impact of summer temperatures (June – August) on the annual glacier mass balance of the TS No.1 glacier system. Importantly, affecting both tree growth and glacier mass balance changes, mean June – August temperature is the common denominator linking both systems, thus allowing us to use precisely dated tree-ring data to reconstruct past glacier dynamics. The temporal resolution of available instrumental GMB records of the TS No.1 glacier covers an annual scale. Hence, using the new LWBI chronology as a predictor, we reconstructed the mean June – August temperature of Tianshan Mountains, and the annual GMB

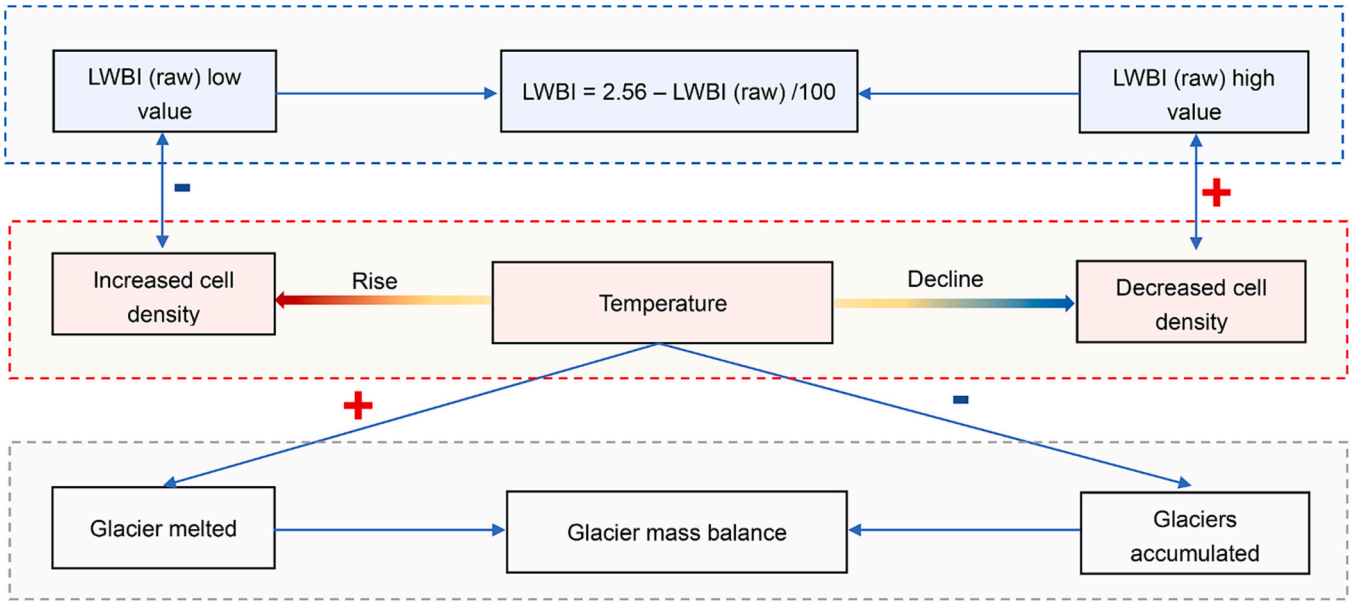

Fig. 9. The relationship between temperature, tree growth and glacier mass balance. +/− indicates positive or negative correlation.

change of the TS No.1 glacier. The following two linear regression models were developed: $T_{6–8} = 9.97\ X_i - 5.45$ and $GMB_{1–12} = -5277.2\ X_i + 4892.6$, where here T6–8 and GMB1–12 are the targets of reconstruction and X is the LWBI index in the year i (Fig. 5a/5b) (Table 3). The reconstruction models explain 41% and 49% of the variance in the raw unfiltered annual GMB and mean summer temperature data, respectively (32% and 35% when both the predictor and predictand are transformed into first-differences). These suggests that the new proxy data can reasonably capture both the long-term trend and the year-to-year variations in the glacier mass balance and temperature. Furthermore, statistical analysis combined with first-order difference and the Durbin-Watson (DW) test indicates no significant positive autocorrelation between the independent variable and the dependent variable (Fig. 5e/5f) (Table 3). Additionally, leave-one-out cross-validation test statistics demonstrate the strength and temporal stability of the two models. The reduction of error (RE) is positive during the validation period, and the sign test yields significant results at the 0.01 level (Table 3).

3.3. Past variations in summer temperature and glacier mass

The full 400-year long temperature and GMB reconstructions are provided in Fig. 6. The mean and standard deviation of the summer temperature record over the past 400 years is 4.49 °C and 0.41 °C respectively, and the mean and standard deviation of the GMB record are −375.83 mm w.e.a^{-1} and 218.56 mm w.e.a^{-1} respectively. Our proxy estimate indicates that for the past four centuries the TS No.1 glacier has been in a state of mass loss for a long time. The warm periods (melt periods) are: 1680–1691, 1698–1714, 1744–1757, 1766–1776, 1791–1810, 1841–1894, 1899–1910, and 1998–2019; and the cold periods (accumulation periods) are: 1660–1679, 1715–1734, 1777–1786, 1829–1840, 1911–1922, 1930–1997 (Fig. 6). Extremely warm years (i.e., years of extreme melt) (mean JJA temperature > 5.32 °C, GMB < −812.95 mm w.e.a^{-1}) are: 1704, 2001, 2010, 2015, 2017, 2018, 2019 (in order of decreasing melt severity); and the extremely cold years (i.e., years of extreme accumulation) (< 3.67 °C , GMB >61.29 mm w.e.a^{-1}) are 1722, 1731, 1779, 1832,1886, 1919, 1920, 1945, 1953, 1957, 1972, 1974, and 1987 (Fig. 6). We identified a total of 43 warm years and 47 cold years, based on the threshold of ±1σ (σ is the standard deviation). The gradual cooling from the late 19th century to the mid-to-late 20th century led to a long-term mass accumulation of the TS No.1 glacier, characterized by frequent extreme (> 61.29 mm w.e.a^{-1}) glacier mass accumulation events. However, after the peak of glacial mass growth in 1974, the TS No.1 glacier faced a rapid mass decline, both in terms of the magnitude and the rate of change, which, in the context of the past 400 years, is unprecedented (Fig. 6b/6c).

Results from the MTM and wavelet power spectrum analysis show that our reconstructed temperature and GMB have interannual, interdecadal, and multi-decadal cyclical characteristics, specifically 2.0–2.3 years (99%), 3.7–4.6 years (95% and 99%), 17.9–18.5 years (95%), 60.2–63.6 years (95%), 144.9–169.4 years (99%), and that this significant periodic change runs through all period (Fig. 7). Spatial correlation analysis against gridded climate data reveal that the LWBI chronology represents the summer temperature variability across a wider region in north-north western China. Additionally, a significant negative correlation is observed between the LWBI chronology and summer mean snow cover in the high latitudes/high altitudes Northern Hemisphere (Fig. 8a/b). The correlation coefficients between the LWBI chronology and the GMB of 76 landmark glaciers in the global glacier mass balance dataset were also calculated (Zemp et al., 2019; Li et al., 2021) (Fig. 8c). The results indicate that over 70% of the 76 global landmark glaciers exhibit a negative relationship with LWBI, indicating widespread melting and mass losses in most glaciers in the northern and southern hemispheres, particularly the high-latitude oceanic glaciers in the northern hemisphere (Fig. 8c).

4. Discussion

4.1. Climate and glacier signals recorded by the latewood blue intensity

Our analysis indicates that the recent decreasing trend in the GMB of the TS No.1 glacier is controlled predominantly by temperature, while the influence of precipitation is limited. The LWBI chronology shows a significant positive correlation with summer temperatures, thus offering a possibility for the indirect use of the BI metric to model changes in the TS No.1 GMB dynamics over the last 400 years. These results are further corroborated by the sensitivity experiment of the latest COSIMA (Coupled Snowpack and Ice surface energy and mass balance model), which confirms that the Tianshan No.1 glacier mass balance is more sensitive to temperature than precipitation, and the mass loss caused by temperature is not compensated by more precipitation (Li et al., 2022). In general, conifers located at high elevation near the tree line are

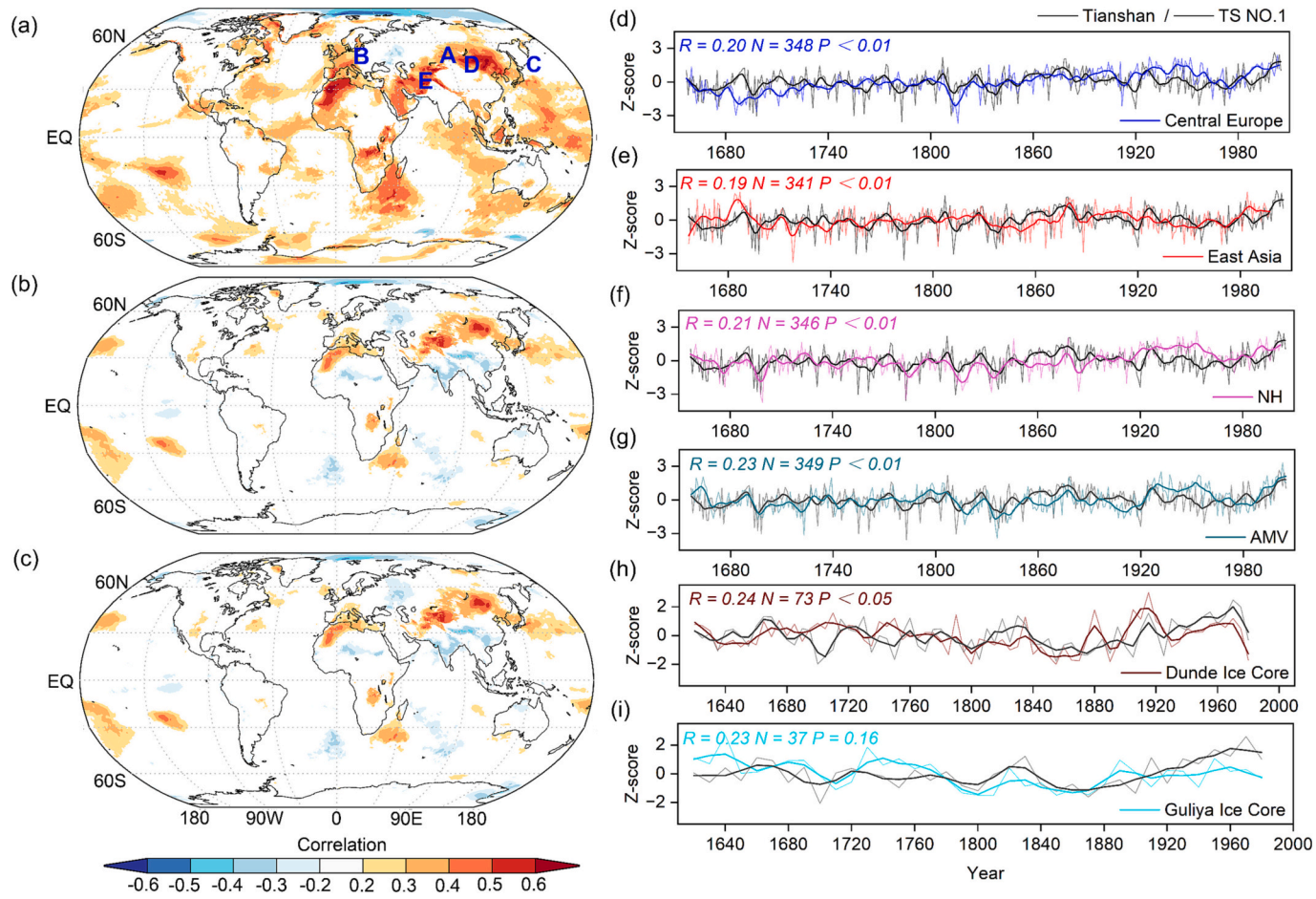

Fig. 10. The spatial correlation analysis of the PC1 and the ERA5 grid temperature dataset after the original (a), detrended (b) and first-order difference (c) calculations in the verification period (1950–2005), all insignificant correlations ($P > 0.05$) were masked out, where A represent the Tianshan Mountains (this study), B represent Central Europe Alps (Büntgen et al., 2006), C represent East Asia (Davi et al., 2002), D represent Dunde ice core (Thompson et al., 2006), and E represent Guliya ice core (Thompson et al., 1997). Comparison of Tianshan temperature reconstruction (PC1) with other MXD-based temperature reconstructions, where (d) is the comparison between PC1 and Central European Alps summer (June to September) temperature reconstruction, (e) is the comparison between PC1 and East Asian Japanese warm season (May to September) temperature reconstruction, and (f) is the comparison between PC1 and Northern Hemisphere summer (June to August) temperature reconstruction (Schneider et al., 2015). (g) is the comparative between the PC1 and Atlantic multidecadal variability (AMV, Wang et al., 2017). Comparison of TS No.1 GMB reconstruction with ice core accumulation data, where (h) is the comparison between TS No.1 GMB reconstruction and Dunde ice core water equivalent net balance (accumulation, 5-year average), (i) is the comparison between TS No.1 GMB reconstruction and Guliya ice core water equivalent net balance (accumulation, 10-year average). All comparison series are *Z*-score normalized and low-pass filtered with a step size of 10 years (ice core accumulation data are 5 year) to achieve low-frequency fluctuations.

sensitive to temperature, and the *Picea schrenkiana* investigated in this study follows this general rule (Yu et al., 2013; Chen et al., 2019b). Xylem cell division and enlargement in conifers are most active during the warmest period of the growing season, and is in this period promoted by earlier snow melting and faster soil warming, leading to faster leaf development, as well as bud and stem growth (Körner, 1998; Alward et al., 1999; Briffa et al., 2001; Peterson and Peterson, 2001; Wilson et al., 2014). Previous research has indicated that the respiration rate of *Picea schrenkiana* increases with high nighttime temperatures, while photosynthesis is not similarly affected by high daytime temperatures (Tian et al., 2017; Jiao et al., 2020; Xue et al., 2022). The higher respiration rates arguably lead to an increased pool of resources to reinforce latewood cell walls, explaining the relationship between high summer temperatures and high latewood density (Björklund et al., 2019), approximated here using the microdensitometric technique of Blue Intensity (Fig. 9).

4.2. Comparison with reconstructed temperature and other glacier records

We perform some comparisons of regional temperature reconstructions based on the maximum latewood density (MXD) parameter in the Tianshan Mountains (Chen et al., 2019b; Yu et al., 2013). The results showed a significant positive relationship between these reconstructions, passing the statistical test ($R_{T-A} = 0.33$, $P < 0.01$; $R_{T-B} = 0.46$, $P < 0.01$), confirming the consistency and reliability of our summer temperature reconstruction in the Tianshan region during the historical period (Fig. 8d). However, differ from the slow warming of the Tianshan Mountain after the 1850s revealed by Chen et al. (2019b), summer temperatures reconstructed by Yu et al. (2013) and ours shows a long-term cooling from 1890 to 1975. These discrepancies may be due to differences in sampling strategy and chronology establishment methods between studies (Cook et al., 2013), such as different sampling heights (about 300 m below our sampling height) and tree growth trend removal methods (the regional curve standardization method), relevant researchers have confirmed that these differences will lead to deviations in the chronologies (Mäkinen and Vanninen, 1999; Helama et al., 2004; Autin et al., 2015). But the range of high and low temperature changes in the east-west direction remains consistent (first order difference, Fig. 8d).

The PC1 (contains 60.5% of the total variance) from the three

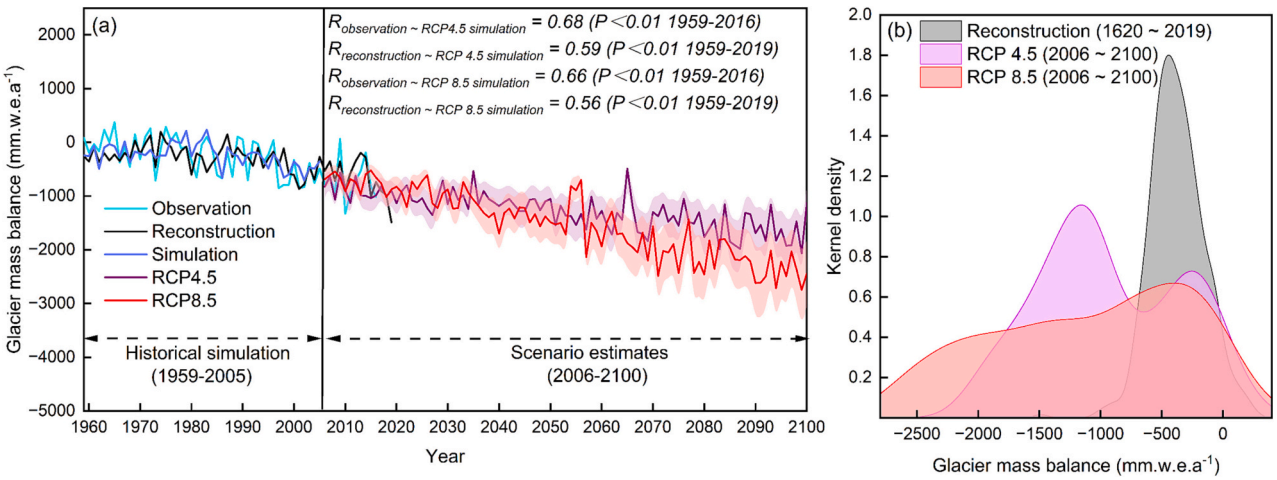

Fig. 11. (a) Observed, reconstructed, and modelled GMB of the TS No.1 glacier. Shaded areas represent the 25%–75% uncertainty intervals. (b) Kernel density distributions of reconstructed (1620–2019 period) and modelled (2006–2100) GMB estimates for the TS No.1 glacier. The latter include the RCP 4.5 and 8.5 scenarios.

temperature reconstructions of the Tianshan mountains (this study, Chen et al., 2019b; Yu et al., 2013) (Fig. 1a) was extracted and compared with temperature records from Central Europe Alps (Büntgen et al., 2006), East Asia (Davi et al., 2002), and the Northern Hemisphere (NH) (Schneider et al., 2015), to evaluate the stability and reliability of the reconstructed Tianshan summer temperature, all comparisons were based on MXD temperature reconstruction (Fig. 10). There is a significant spatial positive correlation between PC1 and mid latitude NH sea/land temperature during the validation period (1950–2005) (Fig. 10). During the historical reconstruction period, some warm/cold periods were co-captured by these records, and PC1 maintained a significant positive correlation with the AMV (r = 0.23, P < 0.01) (Fig. 10g), indicating a common large-scale temperature forcing in the midlatitudes of Eurasia.

To verify the validity of the TS No.1 GMB reconstruction, we compared it with the accumulation data from the Dunde ice core (94.6°E, 39.4°N, Thompson et al., 2006), and Guliya ice core (81.5°E, 35.3°N, Thompson et al., 1997), further to reveal the response of glacier changes in High Mountain Asia to climate change (Duan et al., 2013). As shown in Fig. 10, our GMB reconstructions generally coincide with changes in the net balance of the Dunde and Guliya ice cores, particularly the slow accumulation from 1800 to 1970 and the rapid ablation after the 1970s. These results can verify the reliability of our GMB reconstruction (Fig. 10h and Fig. 10i). With the help of observational data and reconstruction records, we found that most glaciers in the world are rapidly disappearing, but there are still some areas where glaciers show significant growth (Zemp et al., 2019). This inconsistent result can be considered as a heterogeneous response of glacier changes to climate change, that is, the impact of precipitation on glaciers may outweigh that of temperature (Duan et al., 2004). This heterogeneous change poses challenges for regional glacier research, but comparing historical periods with more proxy data can provide longer-term background information (Liu et al., 2021).

4.3. Future changes of Tianshan No.1 glacier under different scenarios

The high-resolution and multi-elements of the East Asian downscaling model (CORDEX-East Asia) data provide an opportunity for us to analysed future climate change (Kim et al., 2021). We selected the CMIP5 HadGEM3 model grid points based on the geographical range of glacier distribution and obtained the monthly mean dataset of 10 meteorological elements to establish a multiple regression model (Jones et al., 2011; Wu et al., 2017). The historical period GMB was fully simulated, and future changes of the GMB under two typical emission paths (RCP 4.5 and RCP 8.5) were predicted. The simulation results indicate that the GMB of TS No.1 glacier continues to decline under both RCP 4.5 and RCP 8.5 scenarios. A comparison between observed and predicted annual GMB shows relatively consistent magnitude and trend in the common period, indicating that the model simulation has a relatively good ability to reproduce and predict GMB changes (Fig. 11a). Correlation analysis further reveals that RCP 4.5 better reproduces GMB changes compared to RCP 8.5, indicating that at the statistical level, the GMB of the TS No.1 glacier may not experience a sharp decline in the near future. However, these are only model predictions and still carry significant uncertainty and challenges (Fig. 11). Nevertheless, when compared to observed or reconstructed GMB data from recent decades or the past or four centuries, the estimated melting of TS No.1 under RCP 4.5 and RCP 8.5 scenarios is unprecedented. In the future, continuous glacier ablation will aggravate the occurrence of meteorological geological disasters such as ice avalanches, flash floods, debris flows, and barrier lakes, cause irreversible damage to the dam power infrastructure (Duan et al., 2013; Duan et al., 2019).

5. Conclusion

In this study, a 525-year latewood blue intensity chronology of *Picea schrenkiana* was developed to reconstruct the summer temperature of the Tianshan and the GMB of the TS No.1 glacier. The reconstruction results indicate that the rapid warming of the Tianshan Mountains since the 1974 accelerated the ablation of the TS No.1 glacier and exceeded the long-term fluctuations of the past 400 years, both in terms of trend and frequency of extreme events. Comparative analysis with other reconstructed temperature and glacier records demonstrates the stability and reliability of our reconstruction, but it also reflects that glacier changes also present complex heterogeneity in historical periods. Model simulations indicate that future persistent warming in the Tianshan Mountains under RCP 4.5 and RCP 8.5 scenarios will lead to continued melting of TS No.1 glacier, which means that we need to adopt more robust mitigation strategies to mitigate the current rapid warming and slow down glaciers melting.

Declaration of Competing Interest

The authors declare that they have no conflict of interest.

Data availability

The data that support the findings of this study are available from the

Mendeley data platform at https://data.mendeley.com/drafts/8yxfjh5ngk

Acknowledgments

This work was supported by the National Natural Science Foundation of China (U1803341, 32061123008), the 2nd Scientific Expedition to the Qinghai-Tibet Plateau (No.2019QZKK010206), and the Scientific Research Fund Project of Yunnan Provincial Department of Education (2022Y060). We thank Shulong Yu from the Institute of Desert Meteorology, China Meteorological Administration for providing temperature reconstruction data for the Tianshan Mountains.

Appendix A. Supplementary data

Supplementary data to this article can be found online at https://doi.org/10.1016/j.gloplacha.2023.104210.

References

Adger, W.N., Huq, S., Brown, K., Conway, D., Hulme, M., 2003. Adaptation to climate change in the developing world. Prog. Dev. Stud. 3 (3), 179–195.
Alward, R.D., Detling, J.K., Milchunas, D.G., 1999. Grassland Vegetation changes and Nocturnal Global Warming. Science 283 (5399), 229–231.
Autin, J., Gennaretti, F., Arseneault, D., Bégin, Y., 2015. Biases in RCS tree ring chronologies due to sampling heights of trees. Dendrochronologia 36, 13–22.
Baek, H.J., Lee, J., Lee, H.S., Hyun, Y.K., Cho, C., Kwon, W.T., Marzin, C., Gan, S.Y., Kim, M.J., Choi, D.H., Lee, J., Lee, J., Boo, K.O., Kang, H.S., Byun, Y.H., 2013. Climate change in the 21st century simulated by HadGEM2-AO under representative concentration pathways. Asia-Pac. J. Atmos. Sci. 49 (5), 603–618.
Biondi, F., Waikul, K., 2004. DENDROCLIM2002: A C++ program for statistical calibration of climate signals in tree-ring chronologies. Comput. Geosci. 30 (3), 303–311.
Björklund, J.A., Gunnarson, B.E., Seftigen, K., Esper, J., Linderholm, H.W., 2014. Blue intensity and density from northern Fennoscandian tree rings, exploring the potential to improve summer temperature reconstructions with earlywood information. Clim. Past 10 (2), 877–885.
Björklund, J., von Arx, G., Nievergelt, D., Wilson, R., Van den Bulcke, J., Günther, B., Loader, N.J., Rydval, M., Fonti, P., Scharnweber, T., Andreu-Hayles, L., Büntgen, U., D'Arrigo, R., Davi, N., De Mil, T., Esper, J., Gärtner, H., Geary, J., Gunnarson, B.E., Hartl, C., Hevia, A., Song, H., Janecka, K., Kaczka, R.J., Kirdyanov, A.V., Kochbeck, M., Liu, Y., Meko, M., Mundo, I., Nicolussi, K., Oelkers, R., Pichler, T., Sánchez-Salguero, R., Schneider, L., Schweingruber, F., Timonen, M., Trouet, V., Van Acker, J., Verstege, A., Villalba, R., Wilmking, M., Frank, D., 2019. Scientific Merits and Analytical challenges of Tree-Ring Densitometry. Rev. Geophys. 57 (4), 1224–1264.
Braithwaite, R.J., 2002. Glacier mass balance: the first 50 years of international monitoring. Prog. Phys. Geograph.: Earth Environ. 26 (1), 76–95.
Briffa, K.R., Osborn, T.J., Schweingruber, F.H., Harris, I.C., Jones, P.D., Shiyatov, S.G., Vaganov, E.A., 2001. Low-frequency temperature variations from a northern tree ring density network. J. Geophys. Res.-Atmos. 106 (D3), 2929–2941.
Buckley, B.M., Hansen, K.G., Griffin, K.L., Schmiege, S., Oelkers, R., D'Arrigo, R.D., Stahle, D.K., Davi, N., Nguyen, T.Q.T., Le, C.N., Wilson, R.J.S., 2018. Blue intensity from a tropical conifer's annual rings for climate reconstruction: An ecophysiological perspective. Dendrochronologia 50, 10–22.
Büntgen, U., Frank, D.C., Nievergelt, D., Esper, J., 2006. Summer temperature variations in the European Alps, AD 755–2004. J. Clim. 19 (21), 5606–5623.
Cao, X., Fang, K., Chen, P., Zhang, P., Björklund, J., Pumijumnong, N., Guo, Z., 2020. Microdensitometric records from humid subtropical China show distinct climate signals in earlywood and latewood. Dendrochronologia 64, 125764.
Cao, X., Hu, H., Kao, P.K., Buckley, B.M., Dong, Z., Chen, X., Zhou, F., Fang, K., 2022. Improved spring temperature reconstruction using earlywood blue intensity in southeastern China. Int. J. Climatol. 42 (12), 6204–6220.
Chen, F., Yuan, Y., Wei, W., Wang, L., Yu, S., Zhang, R., Fan, Z., Shang, H., Zhang, T., Li, Y., 2012. Tree ring density-based summer temperature reconstruction for Zajsan Lake area, East Kazakhstan. Int. J. Climatol. 32 (7), 1089–1097.
Chen, F., Shang, H., Panyushkina, I.P., Meko, D.M., Yu, S., Yuan, Y., Chen, F., 2019a. Tree-ring reconstruction of Lhasa River streamflow reveals 472 years of hydrologic change on southern Tibetan Plateau. J. Hydrol. 572, 169–178.
Chen, F., Yuan, Y., Yu, S., Chen, F., 2019b. A 391-year Summer Temperature Reconstruction of the Tien Shan, reveals Far-reaching Summer Temperature Signals over the Midlatitude Eurasian Continent. J. Geophys. Res.-Atmos. 124 (22), 11850–11862.
Chen, F., Martín, H., Zhao, X., Roig, F., Zhang, H., Wang, S., Yue, W., Chen, Y., 2022a. Abnormally low precipitation-induced ecological imbalance contributed to the fall of the Ming Dynasty: new evidence from tree rings. Clim. Chang. 173 (1), 13.
Chen, F., Yuan, Y., Trouet, V., Büntgen, U., Esper, J., Chen, F., Yu, S., Shen, M., Zhang, R., Shang, H., Chen, Y., Zhang, H., 2022b. Ecological and societal effects of Central Asian streamflow variation over the past eight centuries. npj Climat. Atmosph. Sci. 5 (1), 27.
Cleveland, W.S., Devlin, S.J., 1988. Locally weighted regression: an approach to regression analysis by local fitting. J. Am. Stat. Assoc. 83 (403), 596–610.
Cook, E.R., Briffa, K.R., Meko, D.M., Graybill, D.A., Funkhouser, G., 1995. The'segment length curse'in long tree-ring chronology development for palaeoclimatic studies. The Holocene 5 (2), 229–237.
Cook, E., Krusic, P., Holmes, R., Peters, K., 2005. Program Arstan. Version 1, p. 72.
Cook, E.R., Anchukaitis, K.J., Buckley, B.M., D'Arrigo, R.D., Jacoby, G.C., Wright, W.E., 2010. Asian Monsoon failure and Megadrought during the last Millennium. Science 328 (5977), 486–489.
Cook, E.R., Kairiukstis, L.A., (Eds.)., 2013. Methods of Dendrochronology: Applications in the Environmental Sciences. Springer Science & Business Media.
Davi, N., D'Arrigo, R., Jacoby, G., Buckley, B., Kobayashi, O., 2002. Warm-season annual to decadal temperature variability for Hokkaido, Japan, inferred from maximum latewood density and ring width data. Clim. Chang. 52, 201–217.
Davi, N.K., Rao, M.P., Wilson, R., Andreu-Hayles, L., Oelkers, R., D'Arrigo, R., Nachin, B., Buckley, B., Pederson, N., Leland, C., Suran, B., 2021. Accelerated recent warming and temperature variability over the past eight centuries in the Central Asian Altai from blue intensity in tree rings. Geophys. Res. Lett. 48 (16) e2021GL092933.
Dehecq, A., Gourmelen, N., Gardner, A.S., Brun, F., Goldberg, D., Nienow, P.W., Berthier, E., Vincent, C., Wagnon, P., Trouvé, E., 2019. Twenty-first century glacier slowdown driven by mass loss in High Mountain Asia. Nat. Geosci. 12 (1), 22–27.
Dolgova, E., 2016. June–September temperature reconstruction in the Northern Caucasus based on blue intensity data. Dendrochronologia 39, 17–23.
Duan, K., Yao, T., Thompson, L.G., 2004. Low-frequency of southern Asian monsoon variability using a 295-year record from the Dasuopu ice core in the Central Himalayas. Geophys. Res. Lett. 31, L16209.
Duan, J., Wang, L., Li, L., Sun, Y., 2013. Tree-ring-inferred glacier mass balance variation in southeastern Tibetan Plateau and its linkage with climate variability. Clim. Past 9 (6), 2451–2458.
Duan, J., Ma, Z., Li, L., Zheng, Z., 2019. August-September Temperature Variability on the Tibetan Plateau: past, present, and Future. J. Geophys. Res.-Atmos. 124 (12), 6057–6068.
Dyurgerov, M., 2003. Mountain and subpolar glaciers show an increase in sensitivity to climate warming and intensification of the water cycle. J. Hydrol. 282 (1), 164–176.
Fan, Z.X., Bräuning, A., Yang, B., Cao, K.F., 2009. Tree ring density-based summer temperature reconstruction for the central Hengduan Mountains in southern China. Glob. Planet. Chang. 65 (1), 1–11.
Fritts, H., 1976. Tree Rings and Climate. Elsevier.
Fuentes, M., Salo, R., Björklund, J., Seftigen, K., Zhang, P., Gunnarson, B., Aravena, J.C., Linderholm, H.W., 2018. A 970-year-long summer temperature reconstruction from Rogen, west-Central Sweden, based on blue intensity from tree rings. The Holocene 28 (2), 254–266.
Fujita, K., Nuimura, T., 2011. Spatially heterogeneous wastage of Himalayan glaciers. Proc. Natl. Acad. Sci. 108 (34), 14011–14014.
Gagen, M., McCarroll, D., Loader, N.J., Robertson, I., 2011. Stable Isotopes in Dendroclimatology: moving beyond 'potential'. Dendroclimatology 147–172.
Gao, H., Li, H., Duan, Z., Ren, Z., Meng, X., Pan, X., 2018. Modelling glacier variation and its impact on water resource in the Urumqi Glacier no. 1 in Central Asia. Sci. Total Environ. 644, 1160–1170.
Gou, X., Deng, Y., Gao, L., Chen, F., Cook, E., Yang, M., Zhang, F., 2015. Millennium tree-ring reconstruction of drought variability in the eastern Qilian Mountains, Northwest China. Clim. Dyn. 45 (7), 1761–1770.
Grissino-Mayer, H.D., 2001. Evaluating Crossdating Accuracy: A Manual and Tutorial for the Computer Program COFECHA.
Harley, G.L., Heeter, K.J., Maxwell, J.T., Rayback, S.A., Maxwell, R.S., Reinemann, T.E. P., Taylor, A.H., 2021. Towards broad-scale temperature reconstructions for Eastern North America using blue light intensity from tree rings. Int. J. Climatol. 41 (S1), E3142–E3159.
Harris, I., Jones, P.D., Osborn, T.J., Lister, D.H., 2014. Updated high-resolution grids of monthly climatic observations – the CRU TS3.10 Dataset. Int. J. Climatol. 34 (3), 623–642.
Harris, I., Osborn, T.J., Jones, P., Lister, D., 2020. Version 4 of the CRU TS monthly high-resolution gridded multivariate climate dataset. Sci. Data 7 (1), 1–18.
Heeter, K.J., Harley, G.L., Maxwell, J.T., Wilson, R.J., Abatzoglou, J.T., Rayback, S.A., Rochner, M.L., Kitchens, K.A., 2021a. Summer temperature variability since 1730 CE across the low-to-mid latitudes of western North America from a tree ring blue intensity network. Quat. Sci. Rev. 267, 107064.
Heeter, K.J., Rochner, M.L., Harley, G.L., 2021b. Summer Air Temperature for the Greater Yellowstone Ecoregion (770–2019 CE) over 1,250 years. Geophys. Res. Lett. 48 (7) e2020GL092269.
Helama, S., Lindholm, M., Timonen, M., Eronen, M., 2004. Detection of climate signal in dendrochronological data analysis: a comparison of tree-ring standardization methods. Theor. Appl. Climatol. 79, 239–254.
Jiao, L., Chen, K., Wang, S.J., Liu, X.P., 2020. Stability evaluation of radial growth of Picea schrenkiana in different age groups in response to climate change in the eastern Tianshan Mountains. J. Mt. Sci. 17 (7), 1735–1748.
Joel, D.S., Anne, E.G., 1998. Risks, opportunities, and adaptation to climate change. Clim. Res. 11 (1), 85–95.
Jones, C., Hughes, J.K., Bellouin, N., Hardiman, S.C., Jones, G.S., Knight, J., Zerroukat, M., 2011. The HadGEM2-ES implementation of CMIP5 centennial simulations. Geosci. Model Dev. 4 (3), 543–570.
Kaczka, R.J., Wilson, R., 2021. I-BIND: International Blue intensity network development working group. Dendrochronologia 68, 125859.
Khan, R., Jolly, R., Fatima, T., Shakir, M., 2022. Extraction processes for deriving cellulose: A comprehensive review on green approaches. Polym. Adv. Technol. 33 (7), 2069–2090.

Kim, G., Cha, D.H., Park, C., Jin, C.S., Lee, D.K., Suh, M.S., Oh, S.G., Hong, S.Y., Ahn, J. B., Min, S.K., Kang, H.S., 2021. Evaluation and Projection of Regional climate over East Asia in CORDEX-East Asia phase I Experiment. Asia-Pac. J. Atmos. Sci. 57 (1), 119–134.
Körner, C., 1998. A re-assessment of high elevation treeline positions and their explanation. Oecologia 115 (4), 445–459.
Li, Q., Liu, Y., Nakatsuka, T., Song, H., Mccarroll, D., Yang, Y., Qi, J., 2015. The 225-year precipitation variability inferred from tree-ring records in Shanxi Province, the North China, and its teleconnection with Indian summer monsoon. Glob. Planet. Chang. 132 (sep), 11–19.
Li, Y.J., Ding, Y.J., Shangguan, D.H., Wang, R.J., 2019. Regional differences in global glacier retreat from 1980 to 2015. Adv. Clim. Chang. Res. 10 (4), 203–213.
Larsson, L., 2018. CooRecorder And Cdendro Programs of the CooRecorder/Cdendro Package Version 9.0.1.
Li, Y., Ding, Y., Shangguan, D., Liu, F., Zhao, Q., 2021. Climate-driven acceleration of glacier mass loss on global and regional scales during 1961–2016. Sci. China Earth Sci. 64 (4), 589–599.
Li, H., Wang, P., Li, Z., Jin, S., He, J., 2022. Summertime surface mass balance and energy balance of Urumqi Glacier no. 1, Chinese Tien Shan, modeled by linking COSIMA and in-situ measured meteorological records. Clim. Dyn. 1–23.
Liang, E., Shao, X., Qin, N., 2008. Tree-ring based summer temperature reconstruction for the source region of the Yangtze River on the Tibetan Plateau. Glob. Planet. Chang. 61 (3), 313–320.
Liu, Y., Wang, L., Li, Q., Cai, Q., Song, H., Sun, C., Liu, R., Mei, R., 2019. Asian Summer Monsoon-Related Relative Humidity Recorded by tree Ring $\delta_{18}O$ during last 205 years. J. Geophys. Res.-Atmos. 124 (17–18), 9824–9838.
Liu, Y., Song, H., An, Z., Sun, C., Trouet, V., Cai, Q., Liu, R., Leavitt, S.W., Song, Y., Li, Q., Fang, C., Zhou, W., Yang, Y., Jin, Z., Wang, Y., Sun, J., Mu, X., Lei, Y., Wang, L., Li, X., Ren, M., Cui, L., Zeng, X., 2020. Recent anthropogenic curtailing of Yellow River runoff and sediment load is unprecedented over the past 500 y. Proc. Natl. Acad. Sci. 117 (31), 18251–18257.
Liu, X., Xu, Z., Yang, H., Vaghefi, S.A., 2021. Responses of the glacier mass balance to climate change in the Tibetan Plateau during 1975–2013. J. Geophys. Res.-Atmos. 126 (7) e2019JD032132.
Mäkinen, H., Vanninen, P., 1999. Effect of sample selection on the environmental signal derived from tree-ring series. For. Ecol. Manag. 113 (1), 83–89.
Mann, M.E., Steinman, B.A., Brouillette, D.J., Fernandez, A., Miller, S.K., 2022. On the Estimation of Internal climate Variability during the Preindustrial Past Millennium. Geophys. Geophys. Res. Lett. 49 (2) e2021GL096596.
Martin, G.M., Ringer, M.A., Pope, V.D., Jones, A., Dearden, C., Hinton, T.J., 2006. The Physical Properties of the Atmosphere in the New Hadley Centre Global Environmental Model (HadGEM1). Part I: Model Description and Global Climatology. J. Clim. 19 (7), 1274–1301.
Maxwell, R.S., Hessl, A.E., Cook, E.R., Pederson, N., 2011. A multispecies tree ring reconstruction of Potomac River streamflow (950–2001). Water Resour. Res. 47 (5).
McCabe, G.J., Wolock, D.M., 2010. Long-term variability in Northern Hemisphere snow cover and associations with warmer winters. Clim. Chang. 99 (1), 141–153.
Michaelsen, J., 1987. Cross-validation in statistical climate forecast models. J. Appl. Meteorol. Climatol. 26 (11), 1589–1600.
Osborn, T.J., Biffa, K., Jones, P., 1997. Adjusting variance for sample-size in tree-ring chronologies and other regional mean timeseries. Dendrochronologia 15, 89–99.
Østrem, G., Brugman, M., 1966. Glacier Mass Balance Measurements. Department of Mines and Technical Surveys, Glaciology Section.
Peterson, D.W., Peterson, D.L., 2001. Mountain hemlock growth responds to climatic variability at annual and decadal time scales. Ecology 82 (12), 3330–3345.
Poole, C.F., 2020. Chapter 1 - Milestones in the development of liquid-phase extraction techniques. In: Poole, C.F. (Ed.), Liquid-Phase Extraction. Elsevier, pp. 1–44.
Rabatel, A., Francou, B., Soruco, A., Gomez, J., Cáceres, B., Ceballos, J.L., Basantes, R., Vuille, M., Sicart, J.E., Huggel, C., Scheel, M., Lejeune, Y., Arnaud, Y., Collet, M., Condom, T., Consoli, G., Favier, V., Jomelli, V., Galarraga, R., Ginot, P., Maisincho, L., Mendoza, J., Ménégoz, M., Ramirez, E., Ribstein, P., Suarez, W., Villacis, M., Wagnon, P., 2013. Current state of glaciers in the tropical Andes: a multi-century perspective on glacier evolution and climate change. Cryosphere 7 (1), 81–102.
Radić, V., Hock, R., 2014. Glaciers in the Earth's Hydrological Cycle: Assessments of Glacier Mass and Runoff changes on Global and Regional Scales. Surv. Geophys. 35 (3), 813–837.
Rao, M.P., Cook, E.R., Cook, B.I., D'Arrigo, R.D., Palmer, J.G., Lall, U., Woodhouse, C.A., Buckley, B.M., Uriarte, M., Bishop, D.A., Jian, J., Webster, P.J., 2020. Seven centuries of reconstructed Brahmaputra River discharge demonstrate underestimated high discharge and flood hazard frequency. Nat. Commun. 11 (1), 6017.
Ringer, M.A., Martin, G.M., Greeves, C.Z., Hinton, T.J., James, P.M., Pope, V.D., Scaife, A.A., Stratton, R.A., Inness, P.M., Slingo, J.M., Yang, G.-Y., 2006. The Physical Properties of the Atmosphere in the New Hadley Centre Global Environmental Model (HadGEM1). Part II: Aspects of Variability and Regional climate. J. Clim. 19 (7), 1302–1326.
Rydval, M., Larsson, L.Å., McGlynn, L., Gunnarson, B.E., Loader, N.J., Young, G.H.F., Wilson, R., 2014. Blue intensity for dendroclimatology: should we have the blues? Experiments from Scotland. Dendrochronologia 32 (3), 191–204.
Sakai, A., Fujita, K., 2017. Contrasting glacier responses to recent climate change in high-mountain Asia. Sci. Rep. 7 (1), 13717.
Salzmann, N., Huggel, C., Rohrer, M., Stoffel, M., 2014. Data and knowledge gaps in glacier, snow and related runoff research – A climate change adaptation perspective. J. Hydrol. 518, 225–234.
Schneider, L., Smerdon, J.E., Büntgen, U., Wilson, R.J., Myglan, V.S., Kirdyanov, A.V., Esper, J., 2015. Revising midlatitude summer temperatures back to AD 600 based on a wood density network. Geophys. Res. Lett. 42 (11), 4556–4562.
Schweingruber, F.H., 2012. Tree Rings: Basics and Applications of Dendrochronology. Springer Science & Business Media.
Seftigen, K., Fuentes, M., Ljungqvist, F.C., Björklund, J., 2020. Using Blue Intensity from drought-sensitive Pinus sylvestris in Fennoscandia to improve reconstruction of past hydroclimate variability. Clim. Dyn. 55 (3), 579–594.
Shi, Y., Shen, Y., Kang, E., Li, D., Ding, Y., Zhang, G., Hu, R., 2007. Recent and Future climate Change in Northwest China. Clim. Chang. 80 (3), 379–393.
Simpson, N.P., Mach, K.J., Constable, A., Hess, J., Hogarth, R., Howden, M., Lawrence, J., Lempert, R.J., Muccione, V., Mackey, B., New, M.G., O'Neill, B., Otto, F., Pörtner, H.O., Reisinger, A., Roberts, D., Schmidt, D.N., Seneviratne, S., Strongin, S., van Aalst, M., Totin, E., Trisos, C.H., 2021. A framework for complex climate change risk assessment. One Earth 4 (4), 489–501.
Soares dos Santos, T., Mendes, D., Rodrigues, Torres R., 2016. Artificial neural networks and multiple linear regression model using principal components to estimate rainfall over South America. Nonlinear Process. Geophys. 23 (1), 13–20.
Speer, J.H., 2010. Fundamentals of Tree-Ring Research. University of Arizona Press.
Thompson, L.G., Yao, T., Davis, M.E., Henderson, K.A., Mosley-Thompson, E., Lin, P.N., Beer, J., Synal, H.A., Cole-dai, J., Bolzan, J.F., 1997. Tropical climate instability: the last glacial cycle from a Qinghai-Tibetan ice core. science 276 (5320), 1821–1825.
Thompson, L.G., Mosley-Thompson, E., Brecher, H., Davis, M., Leon, B., Les, D., Lin, P.N., Mashiotta, T., Mountain, K., 2006. Abrupt tropical climate change: past and present. Proc. Natl. Acad. Sci. 103 (28), 10536–10543.
Tian, Q., He, Z., Xiao, S., Peng, X., Ding, A., Lin, P., 2017. Response of stem radial growth of Qinghai spruce (Picea crassifolia) to environmental factors in the Qilian Mountains of China. Dendrochronologia 44, 76–83.
Tsvetanov, N., Dolgova, E., Panayotov, M., 2020. First measurements of Blue intensity from Pinus peuce and Pinus heldreichii tree rings and potential for climate reconstructions. Dendrochronologia 60, 125681.
Unger-Shayesteh, K., Vorogushyn, S., Farinotti, D., Gafurov, A., Duethmann, D., Mandychev, A., Merz, B., 2013. What do we know about past changes in the water cycle of Central Asian headwaters? A review. Glob. Planet. Chang. 110, 4–25.
van Vuuren, D.P., Stehfest, E., den Elzen, M.G.J., Kram, T., van Vliet, J., Deetman, S., Isaac, M., Klein, Goldewijk K., Hof, A., Mendoza, Beltran A., Oostenrijk, R., van Ruijven, B., 2011. RCP2.6: exploring the possibility to keep global mean temperature increase below 2°C. Clim. Chang. 109 (1), 95.
Wang, X., Siegert, F., Zhou, A.G., Franke, J., 2013. Glacier and glacial lake changes and their relationship in the context of climate change, Central Tibetan Plateau 1972–2010. Glob. Planet. Chang. 111, 246–257.
Wang, P., Li, Z., Li, H., Wang, W., Yao, H., 2014. Comparison of glaciological and geodetic mass balance at Urumqi Glacier no. 1, Tian Shan, Central Asia. Glob. Planet. Chang. 114, 14–22.
Wang, J., Yang, B., Ljungqvist, F.C., Luterbacher, J., Osborn, T.J., Briffa, K.R., Zorita, E., 2017. Internal and external forcing of multidecadal Atlantic climate variability over the past 1,200 years. Nat. Geosci. 10 (7), 512–517.
Wang, R., Liu, S., Shangguan, D., Radić, V., Zhang, Y., 2019. Spatial Heterogeneity in Glacier Mass-Balance Sensitivity across High Mountain Asia. Water 11 (4), 776.
Wang, F., Arseneault, D., Boucher, É., Yu, S., Ouellet, S., Chaillou, G., Delwaide, A., Wang, L., 2020. Chemical destaining and the delta correction for blue intensity measurements of stained lake subfossil trees. Biogeosciences 17 (18), 4559–4570.
Wigley, T.M., Briffa, K.R., Jones, P.D., 1984. On the average value of correlated time series, with applications in dendroclimatology and hydrometeorology. J. Appl. Meteorol. Climatol. 23 (2), 201–213.
Wilson, R., Rao, R., Rydval, M., Wood, C., Larsson, L.-Å., Luckman, B.H., 2014. Blue Intensity for dendroclimatology: the BC blues: A case study from British Columbia, Canada. The Holocene 24 (11), 1428–1438.
Wilson, R., Wilson, D., Rydval, M., Crone, A., Büntgen, U., Clark, S., Ehmer, J., Forbes, E., Fuentes, M., Gunnarson, B.E., Linderholm, H.W., Nicolussi, K., Wood, C., Mills, C., 2017. Facilitating tree-ring dating of historic conifer timbers using Blue Intensity. J. Archaeol. Sci. 78, 99–111.
Wu, Z., Chen, X., Lu, G., Xiao, H., He, H., Zhang, J., 2017. Regional response of runoff in CMIP5 multi-model climate projections of Jiangsu Province, China. Stoch. Env. Res. Risk A. 31 (10), 2627–2643.
Xiao, Y., Shangguan, D., 2018. The dataset of global glacier monitoring mass balance (Version 1.0) (1950–2016). In: National Tibetan Plateau/Third Pole Environment Data Center. https://doi.org/10.11888/Glacio.tpdc.270049. CSTR:18406.11.Glacio.tpdc.270049.
Xue, R., Jiao, L., Qi, C., Chen, K., Liu, X., Du, D., Wu, X., 2022. Growth and response patterns of Picea crassifolia and Pinus tabuliformis to climate factors in the Qilian Mountains, Northwest China. Dendrochronologia 71, 125905.
Yang, B., Qin, C., Wang, J., He, M., Melvin, T.M., Osborn, T.J., Briffa, K.R., 2014. A 3,500-year tree-ring record of annual precipitation on the northeastern Tibetan Plateau. Proc. Natl. Acad. Sci. 111 (8), 2903.
Yang, M., Wang, X., Pang, G., Wan, G., Liu, Z., 2019. The Tibetan Plateau cryosphere: Observations and model simulations for current status and recent changes. Earth Sci. Rev. 190, 353–369.
Yu, S., Yuan, Y., Wei, W., Chen, F., Zhang, T., Shang, H., Zhang, R., Qing, L., 2013. A 352-year record of summer temperature reconstruction in the western Tianshan Mountains, China, as deduced from tree-ring density. Quat. Res. 80 (2), 158–166.
Yue, X., Zhao, J.U.N., Li, Z., Zhang, M., Fan, J.I.N., Wang, L., Wang, P., 2017. Spatial and temporal variations of the surface albedo and other factors influencing Urumqi Glacier no. 1 in Tien Shan, China. J. Glaciol. 63 (241), 899–911.

Zemp, M., Hoelzle, M., Haeberli, W., 2009. Six decades of glacier mass-balance observations: a review of the worldwide monitoring network. Ann. Glaciol. 50 (50), 101–111.
Zemp, M., Huss, M., Thibert, E., Eckert, N., McNabb, R., Huber, J., Barandun, M., Machguth, H., Nussbaumer, S.U., Gärtner-Roer, I., Thomson, L., Paul, F., Maussion, F., Kutuzov, S., Cogley, J.G., 2019. Global glacier mass changes and their contributions to sea-level rise from 1961 to 2016. Nature 568 (7752), 382–386.
Zhang, R., Wei, W., Shang, H., Yu, S., Gou, X., Qin, L., Bolatov, K., Mambetov, B.T., 2019. A tree ring-based record of annual mass balance changes for the TS.Tuyuksuyskiy Glacier and its linkages to climate change in the Tianshan Mountains. Quat. Sci. Rev. 205, 10–21.